Auto-disturbance rejection controller for novel planar switched reluctance motor

J.F. Pan, N.C. Cheung and J.M. Yang

Abstract: A novel planar motor based on the switched reluctance (SR) principle has been developed. This motor has the advantages of simple structure, low cost and ease of manufacture. The motor is highly reliable and can work in hostile working environments. However, in many industrial applications, the motor's performance is subject to practical constraints, such as mechanical noise, load disturbance and friction. The motor cannot cope with these difficulties under classical PID control scheme. Therefore an auto-disturbance rejection control (ADRC) strategy is proposed to overcome these problems. An ADRC velocity control strategy is implemented on the planar motor, and its performance is then compared with a classical PID controller. Experiment results demonstrate that the motor is more resistant to disturbances under this new control scheme. It confirms that ADRC is an effective solution to overcome the inherent control problems of the SR planar motor. It is expected that the same method can be applied to other SR machines with the same promising results.

1 Introduction

Direct-drive machines have the advantages of simple structure, reduced mechanical parts, high speed and high precision [1]. However, some of the benefits associated with mechanical transmission, such as the ability to reduce model uncertainties and external disturbances, are lost. Therefore, it is of great importance to employ a suitable control algorithm to compensate for the unpredictable changes as much as possible.

In [2], a novel planar motor based on switched reluctance principle was proposed. This machine has simple mechanical structure, and it is very suitable for mass production. In addition, the dimensions of the base plate can easily be altered to fit various application requirements. Figure 1 shows the overall structure of the planar SR motor. The mechanical structure is based on the 'straightened-out' version of a 6/4-pole rotary switched reluctance motor, along the x- and y-axes. The mover coils are arranged as the two same movers of linear motors intercross with each other and each direction of movement has three coils. The stator plate consists of square extrusion blocks to facilitate magnetic paths in two dimensions. Each axis has a pair of linear guides to support the motor's movements. Table 1 shows some of the motor parameters.

During the initial development stage, the planar motor is implemented using the PID control method [3] with a two dimensional lookup table to smooth out the nonlinear force behaviour of the SR planar motor [4]. Under this condition, the planar motor has achieved a position accuracy of several micrometres along the x and y directions. In general, PID control originates from process control strategy, where the controller makes decisions according to the error information. It does not rely on a detailed mathematical model of the motor. However, PID control is insufficient to control the SR planar motor, for the following reasons:

1 Derivative signal noise: Sometimes the reference signal cannot be differentiated or the derivatives are hard to retrieve or the actual output signal is populated by noise. Therefore, the differential signals from the difference between actual and reference signal may be distorted or the noise might be amplified from the output of a classical differentiator.

2 Treatment of different error behaviours – past $\left(\int e dt\right)$, present (e) and future (de/dt). In a typical PID controller, the different error states (past, present and future) are combined by simple linear summations with weighting factors K_p, K_d and K_i. This can unavoidably lead to the conflict between response time and overshoot [5] for this planar motor.

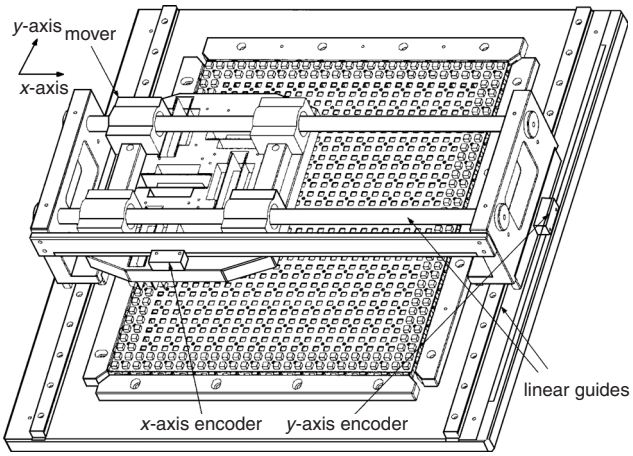

Fig. 1 *Overall structure of planar SR motor*

IEE Proceedings online no. 20050077

doi:10.1049/ip-epa:20050077

Paper first received 8th March 2005 and in final revised form 2nd September 2005

J.F. Pan and N.C. Cheung are with the Department of Electrical Engineering, Hong Kong Polytechnic University, Hong Kong, People's Republic of China

J.M. Yang is with the Electrical Power College, South China University of Technology, Guangzhou, People's Republic of China

E-mail: eencheun@polyu.edu.hk

Table 1: Planar motor specifications

Pole pitch	6 mm
Airgap	0.55 mm
Number of turns per phase	160
Rate power	120 W
Phase resistance	1.5 Ω
Size of base plate	450 × 450 mm
Travel distance	300 × 300 mm
Mover size	250 × 220 mm
Encoder precision	0.5 μm

To combat the problems inherent in PID control of this planar motor, this paper presents a novel control strategy based on the auto-disturbance rejection control (ADRC) scheme. The ADRC concept is derived from the idea of using nonlinear feedback configuration based on process control strategy. It is initially applied to industrial applications such as time-variant, highly-coupled systems [6, 7]. Because it does not rely on exact mathematical model and the whole disturbance including model inconsistency together with outside disturbance can be compensated for, the interest of applications in the motion control area is increasing. Past work proves its successful implementation on permanent magnetic motors [8, 9] and induction motors [10]; it can also be applied to different kinds of motion systems with satisfactory results [11, 12]. Moreover, an ADRC control scheme is more suitable than a PID controller for this type of motor, since the unmodelled parameter variations and external disturbances can be observed and compensated for by the control system in real-time. Therefore, the motor is much more robust and more resistant to external disturbances. So far, there has been no relevant article discussing implementation of the new control method on a switched reluctance machine. In the work described in this paper, the authors have successfully implemented this strategy onto speed regulation of the specialised planar SR motor and experimental results show the distinct performances from an ADRC compared with a typical PID controller; therefore this control algorithm has the potential usage for more industrial SR applications.

2 ADRC

A typical ADRC controller is shown in Fig. 2 and it consists of the following parts:

(*a*) tracking differentiator (TD)

(*b*) nonlinear state error feedback (NLSEF)

(*c*) extended state observer (ESO).

The tracking differentiator is responsible for the arrangement of an appropriate transient process and provides proper differential signals of each order from the input

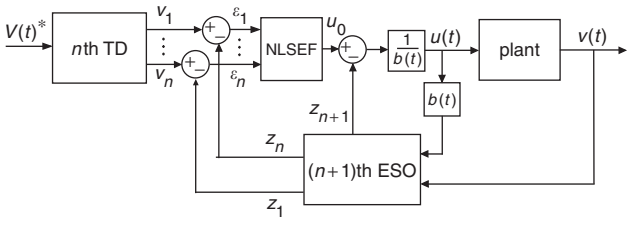

Fig. 2 *ADRC control block*

reference signal. The NLSEF block determines control input by tracking the error signal and its different formats for optimal combinations with nonlinear algorithms for output. The core for an ADRC controller is ESO, which is capable of observing system uncertainties and external disturbances and providing feedback for compensation. Figure 2 shows a general *n*th order ADRC control block.

2.1 Tracking differentiator (TD)

In motor control systems, the differential signal is usually obtained by backward difference of the given signal, such as position. Unavoidably, it will contain a certain amount of stochastic noise. TD can resolve the problem of differential signal extraction via integration. A detailed description of a tracking differentiator can be found in [5, 13].

A dynamic system can be described by the following set of equations:

$$\begin{cases} \dot{x}_1 = x_2 \\ \dot{x}_2 = -g(x_1, x_2) \end{cases} \tag{1}$$

If the system is stable at origin, then for any bounded integrals function $v(t)$, $t \in [0, \infty)$ there exists

$$\begin{cases} \dot{x}_1 = x_2 \\ \dot{x}_2 = R^2 g(x_1 - v(t),\ x_2/R) \end{cases} \tag{2}$$

that satisfies, $\lim_{R\to\infty} \int_0^T |x_1(R,t) - v(t)|dt = 0$. x_1 tracks reference $v(t)$, and $x_2(R,t)$ approximates to the 'generalised differentiation' of $v(t)$ [13]. As long as R is sufficiently large, x_1 can track $v(t)$ arbitrarily fast with certain precision.

Generally a second-order TD takes the following form:

$$\begin{cases} \varepsilon_0 = v_1 - v^* \\ \dot{v}_1 = -r^* fal(\varepsilon_0, a_0, \delta_0) \end{cases} \tag{3}$$

where v^* is the reference velocity, v_1 is its tracking signal, r, a_0 and δ_0 are parameters to be regulated. The *fal* function is expressed as

$$fal(\varepsilon, a, \delta) = \begin{cases} |\varepsilon|^a \operatorname{sgn}(\varepsilon), & |\varepsilon| > \delta \\ \dfrac{\varepsilon}{\delta^{1-a}}, & |\varepsilon| \le \delta \end{cases} \tag{4}$$

The most important feature of TD is its capability to obtain the derivatives of noisy signals with a good signal-to-noise ratio and the derivatives are acquired via integration [5]. Therefore, TD can avoid unnecessary noise and can also be used as a reference generator.

2.2 Nonlinear state error feedback (NLSEF)

A typical PID controller simply takes the linear summations with weighting factors as the controller output, which is problem oriented and difficult for repeatability of different problems [5, 14], whereas in an ADRC the errors are combined with nonlinear manners and the parameters can be regulated according to actual response of output performances.

A typical nonlinear relationship for an *n*th NLSEF can be expressed as

$$u_0 = k_1 fal(\varepsilon_1, \alpha, \delta) + \cdots + k_n fal(\varepsilon_n, \alpha, \delta) \tag{5}$$

where k_1, α and δ are parameters to be regulated. ε_1 is the error signal and its derivatives are obtained from an *n*th-order TD. The *fal* function is derived from (4). The reason why a nonlinear combination of error signals over a linear one can be explained from the graphic interpretation in Fig. 3.

Figure 3 shows that, at higher gains, error is relatively small; at lower gains the error becomes larger. This observation corresponds to intuitive knowledge in practice;

however, the gain remains uniformly the same in the linear gain combination method. Furthermore, from the graphical illustration, there is a linear region in which the error ε falls into the intervals of $\pm\delta$ while the error is getting larger and the gain diminishes accordingly. This avoids excessive gain when the error is small, which might lead to high-frequency chattering [5, 13, 14] of the planar motor.

2.3 ESO

The observer construction is derived from the problem that for a system with the expression:

$$a(t) = f(x, \dot{x}, \ldots, x^{(n-1)}(t), t) + u(t) \tag{6}$$

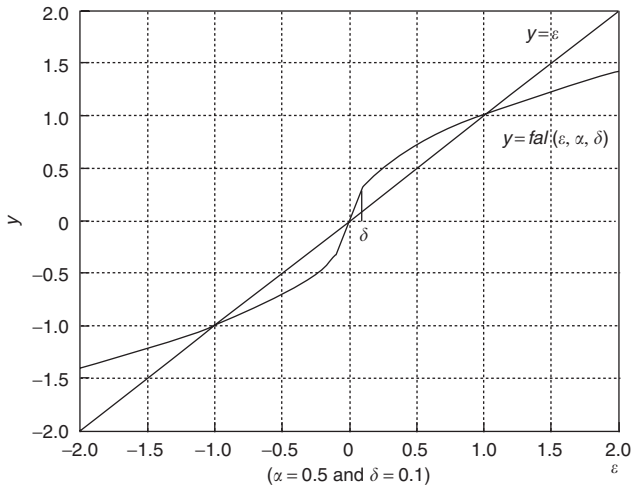

Fig. 3 *Comparison of linear and nonlinear gains*

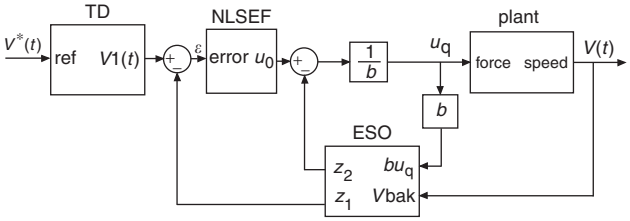

Fig. 4 *ADRC scheme for velocity control loop*

where $f(x, \dot{x}, \ldots, x^{(n-1)}, t)$ is an unknown function and $u(t)$ is the unknown disturbance, the method to construct a nonlinear system which is independent of $f(x, \dot{x}, \ldots, x^{(n-1)}, t)$ and $u(t)$, and enable the system to observe each state variable $x(t) \ldots x^{(n-1)}(t)$, can be realised as follows [15]:

First assume that the solution to the above problem exists, therefore we can obtain the following nonlinear system:

$$\begin{cases} \varepsilon = z_1 - x(t) \\ \dot{z}_1 = z_2 - g_1(\varepsilon) \\ \dot{z}_2 = z_3 - g_2(\varepsilon) \\ \vdots \\ \dot{z}_{n+1} = -g_{n+1}(\varepsilon) \end{cases} \tag{7}$$

The system can satisfy the condition that, for each state (from z_1 to z_{n+1}), it can track corresponding input states correctly, so that $z_1(t) \to x(t) \ldots \ldots z_{n+1}(t) \to x^{(n)}(t)$. If the above statement is true, and we assign $a(t) = f(x, \dot{x}, \ldots, x^{(n-1)}(t), t) + u(t)$, we can get $z_{n+1}(t) \to x^{(n)}(t) = a(t)$. This means that despite the unknown formats for both $f(x, \dot{x}, \ldots, x^{(n-1)}, t)$ and $u(t)$, the real-time value of $a(t)$ can be observed and estimated. Now we can focus on the possibilities for construction of such a system [15]. Let $x_1(t) = x(t) \ldots \ldots x_{n+1}(t) = a(t)$, then system (7) becomes:

$$\begin{cases} \dot{x}_1(t) = x_2(t) \\ \dot{x}_2(t) = x_3(t) \\ \vdots \\ \dot{x}_n(t) = x_{n+1}(t) \\ \dot{x}_{n+1}(t) = b(t) \end{cases} \tag{8}$$

Now let $\delta x_1 = z_1 - x_1(t) \cdots\cdots \delta x_{n+1} = z_{n+1} - x_{n+1}(t)$, then

$$\begin{cases} \dot{\delta}x_1 = \delta x_2 - g_1(\delta x_1) \\ \dot{\delta}x_2 = \delta x_3 - g_2(\delta x_1) \\ \vdots \\ \dot{\delta}x_{n+1} = -b(t) - g_{n+1}(\delta x_1) \end{cases} \tag{9}$$

For any values of $b(t)$ within a certain range, proper functions $g_1(\delta x_1), \ldots\ldots, g_{n+1}(\delta x_1)$ can be selected to make system (9) stable at origin. System (9) is called the 'extended

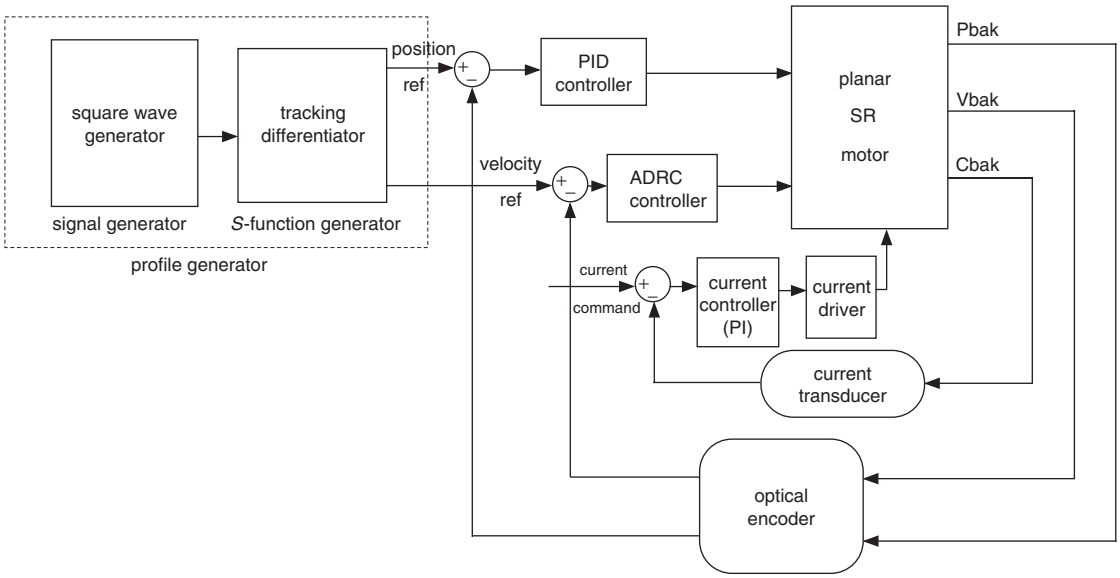

Fig. 5 *Whole control diagram of controller*

state observer' such that besides all system states to be observed, Z_1–Z_n, the state of both the parameter uncertainties and the external disturbances (the extended state) can also be estimated. The convergence derivation of TD and ESO can be found in [13, 15].

Different forms of $g(x)$ can be selected according to different requirements. In our experiment, the *fal* function is chosen. It is obvious that the system is the classical Luenberger observer when $gx_i = x_i\,(i = 1 \ldots n+1)$ and is a variable structure observer when $gx_i = x_i + k_i sign(x_i)$ $(i = 1 \ldots n+1)$ [16].

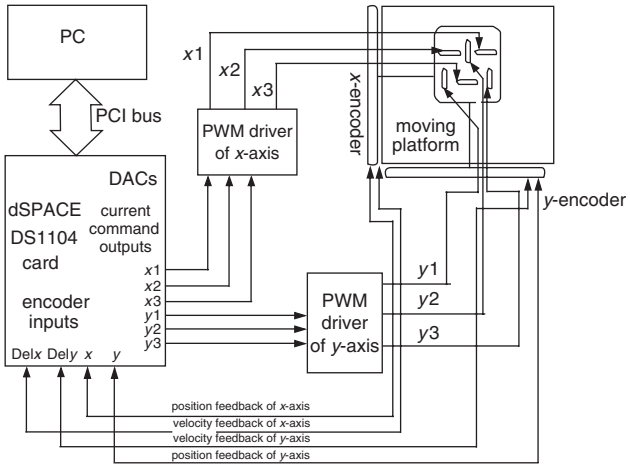

Fig. 6 *Overall experiment setup*

3 Construction of ADRC controller

For switched reluctance motors, the external disturbances may include the change of load or friction. For parameter uncertainties, there maybe (*a*) change of mechanical parameters such as mass (M) and friction coefficient (B_v), and (*b*) electrical, change of winding resistance (R) or control signal fluctuation such as force or current ripples.

The force equation of the planar motor (one-axis) can be represented as

$$M\dot{V} + B_v V + f_l(t) = \sum_{k=a}^{c} f_k(i_k(t), x(t)) = u_q \qquad (10)$$

where $f_{x(y)}$ is the totally generated electromechanical force, $f_l(t)$ is load force, and M, B_v are the mass and the friction constant, respectively. If disturbances and uncertainties are concerned, then the equation becomes

$$\dot{V} = (\Delta B + B_m)V + (\Delta A + A_m)f_l + (\Delta A + A_m)u_q \quad (11)$$

where $B_m = -B_v/M$, $A_m = -1/M$ and ΔB, ΔA are parameter variations. The equation can be further

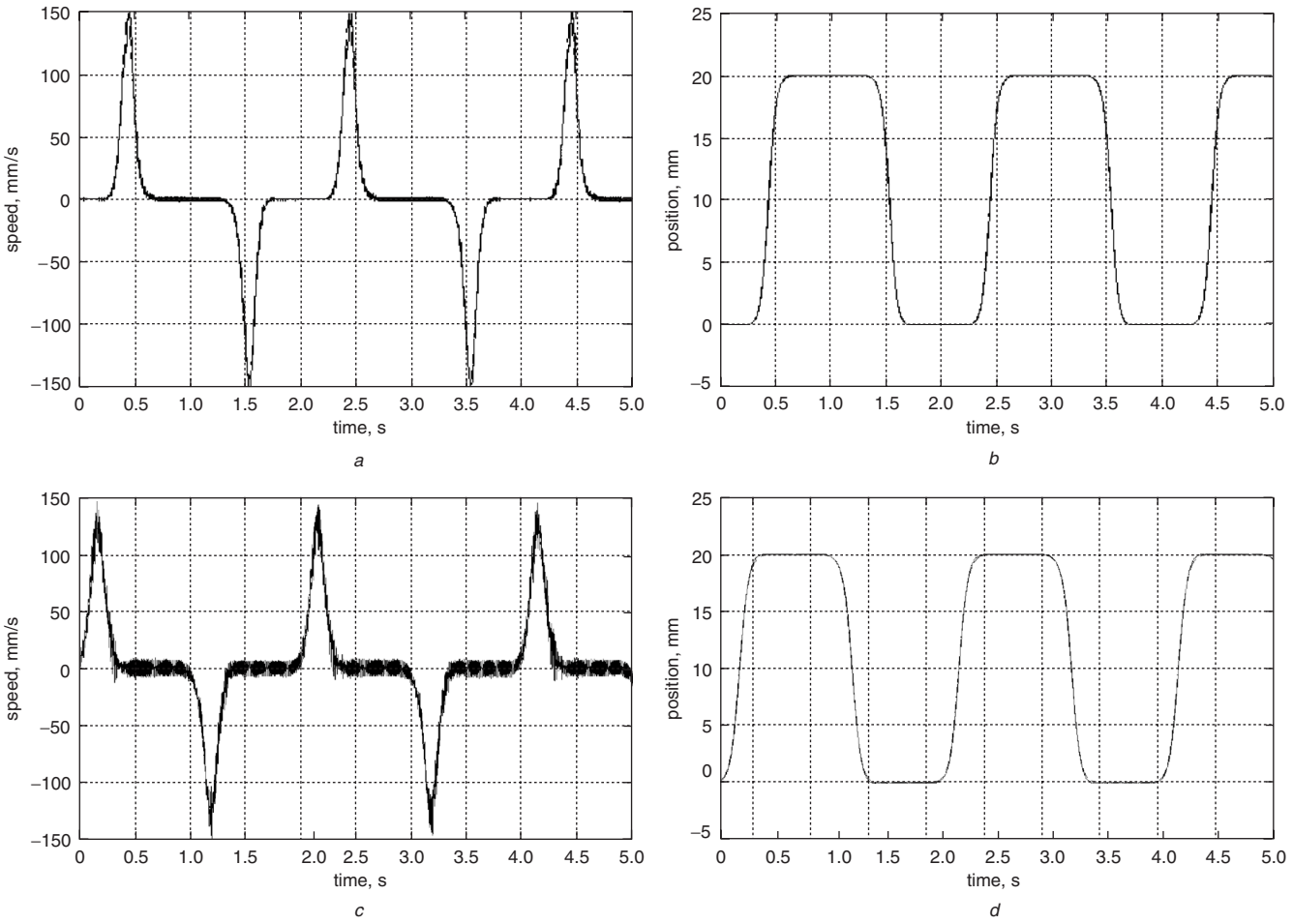

Fig. 7 *Responses of PID controller under 0.5 Hz, 20 mm trajectory profile*
a Velocity response of *x*-axis
b Position response of *x*-axis
c Velocity response of *y*-axis
d Position response of *y*-axis

Table 2: Parameter regulations

PID				ADRC									
				TD (14)			ESO (17)				NLSEF (15)		
x	P	D	I	r_T	a_T	δ_T	B01_E	B02_E	a_E	δ_E	B1_N	a_N	δ_N
	42	2.5	0.2	3000	0.9	0.8	800	150	0.2	0.1	150	0.5	0.01
y	P	D	I	r_T	a_T	δ_T	B01_E	B02_E	a_E	δ_E	B1_N	a_N	δ_N
	60	4	0.1	5000	0.9	0.9	1500	100	0.1	0.1	100	0.9	0.01

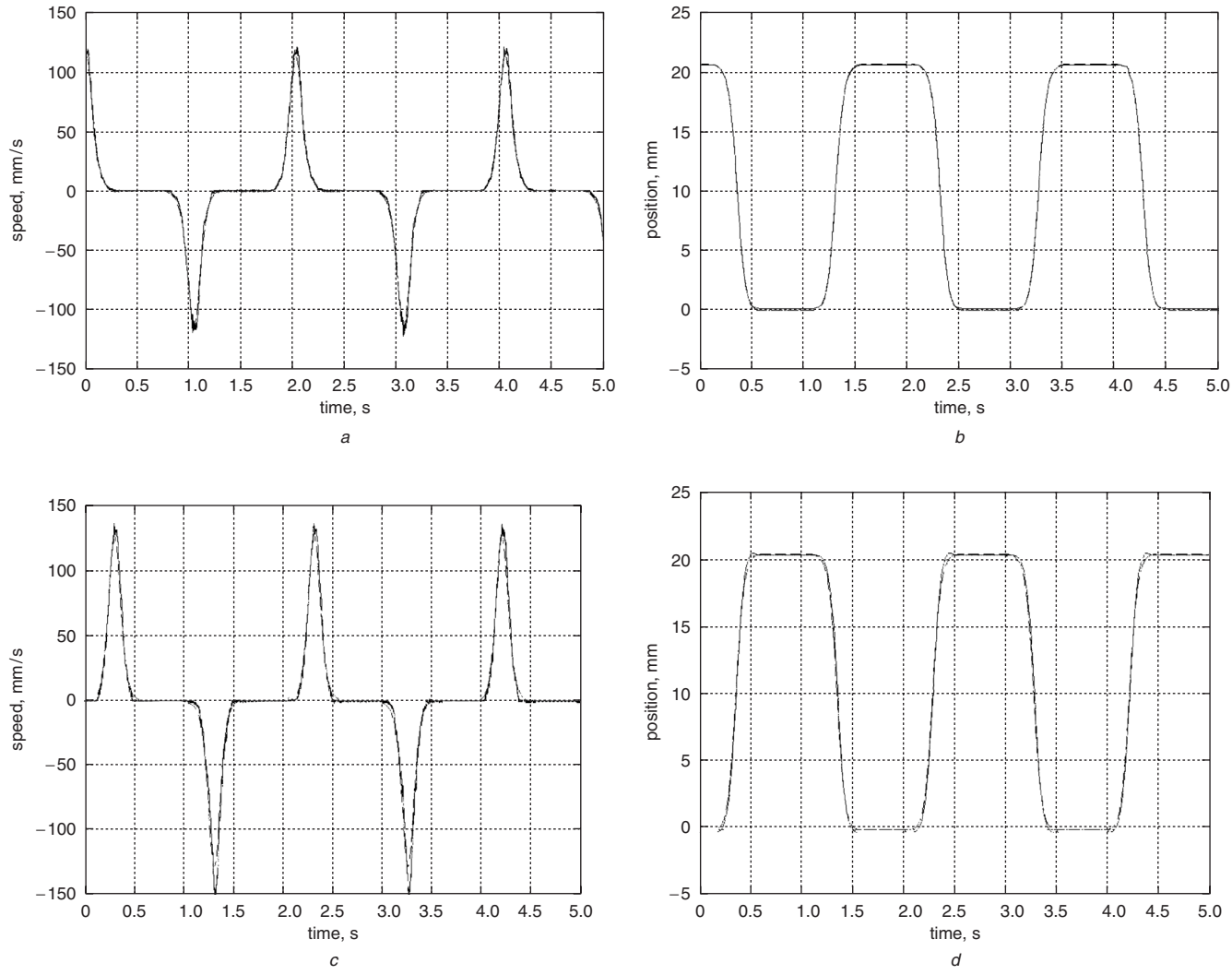

Fig. 8 *Responses of ADRC controller under 0.5 Hz, 20 mm trajectory profile*
a Velocity response of *x*-axis
b Position response of *x*-axis
c Velocity response of *y*-axis
d Position response of *y*-axis

represented as:

$$\begin{aligned}\dot{V} &= F_w + B_m V + A_m u_q \\ &= F_w - \frac{B_v}{M} V + \frac{1}{M} u_q \\ &= a(t) + b u_q \end{aligned} \tag{12}$$

where (i) $F_w = \Delta B V + (\Delta A + A_m) f_l + \Delta A u_q$ which includes all external disturbances and system uncertainties; and (ii) $b = 1/M$ and $a(t) = F_w - \frac{B_v}{M} V$.

The above differential equation for velocity includes only (i) the compositive uncertainties $a(t)$ and (ii) the control parameter bu_q. Therefore, if the compositive item can be observed correctly by ADRC and fed back to the system, the model of this SR motor (one-axis) becomes a first-order system. Also, the other axis can be treated in the same way since the two axes of motion are highly decoupled [4]. Thus, the controller for the system can be expressed as

$$u(t) = (u_0(t) - a(t))/b \tag{13}$$

where $a(t)$ is the observation of total uncertainties and disturbances from the ESO. Since each axis of motion is perfectly decoupled, the controllers for *x*- and *y*-axis can be designed individually. The differences between the two directions are mainly mover mass and friction. Therefore, after a controller of one axis of motion is designed, the one

for another motion can be obtained with only slight modifications.

The control object is focused on velocity. Take x-axis of motion for example. The input for TD is speed command and it will arrange a proper transient process which has the output of TD of

$$V_1(t) = -r\_Tx\, fal(V_1 - V, \delta\_Tx, \alpha\_Tx) \tag{14}$$

where r_Tx, δ_Tx and α_Tx are parameters for the tracking differentiator to be regulated. Then the output V_1 is compared with observed speed state fed back from the ESO, the difference is determined by the NLSEF block to give a proper u_0:

$$u_0 = \beta\_Nx\, fal(\varepsilon, \delta\_Nx, \alpha\_Nx) \tag{15}$$

Three more regulated values β_Nx, δ_Nx and α_Nx are included. Then the control force input u_q for the motor becomes

$$u_q = \frac{1}{b}(u_0 - Z_2) \tag{16}$$

where b is a constant and $b = 1/M$. The actual measured velocity value from the encoder will be fed back to the ESO for state observation; the velocity state Z_1 and the extended state Z_2 are derived from the following:

$$\begin{cases} \dot{Z}_1 = bu_q + Z_2 - \beta_{01\_EX}\, fal(Z_1 - V_{bak}, \delta_{EX}, \alpha_{EX}) \\ \dot{Z}_2 = -\beta_{02\_EX}\, fal(Z_1 - V_{bak}, \delta_{EX}, \alpha_{EX}) \end{cases} \tag{17}$$

Again, four parameters β_{01_EX}, β_{02_EX}, δ_{EX} and α_{EX} to be regulated are introduced. The whole control block can be derived from the above and is shown in Fig. 4 (the subscripts Tx, EX and Nx stand for parameters for the TD, ESO and NLSEF of the x-axis).

The ADRC parameters are obtained from simulation and experimental results. As well as this, the following steps should be observed: first, according to the characteristics of the control object, system stability should be ensured. Then, the parameters of TD and ESO are regulated to evaluate the reference inputs, the variables of each state and the disturbances, quickly and correctly. Afterwards, the NLSEF parameters are also adjusted to conform to the closed-loop performance requirements.

Since the two axes of the motor are decoupled from each other, we can consider the x- and y-axis individually. First, by using the combined force command from the ADRC controller, the controller will decide which operating region the motor is in. Then, according to the mover's position and required force, the excitation force for each phase is calculated.

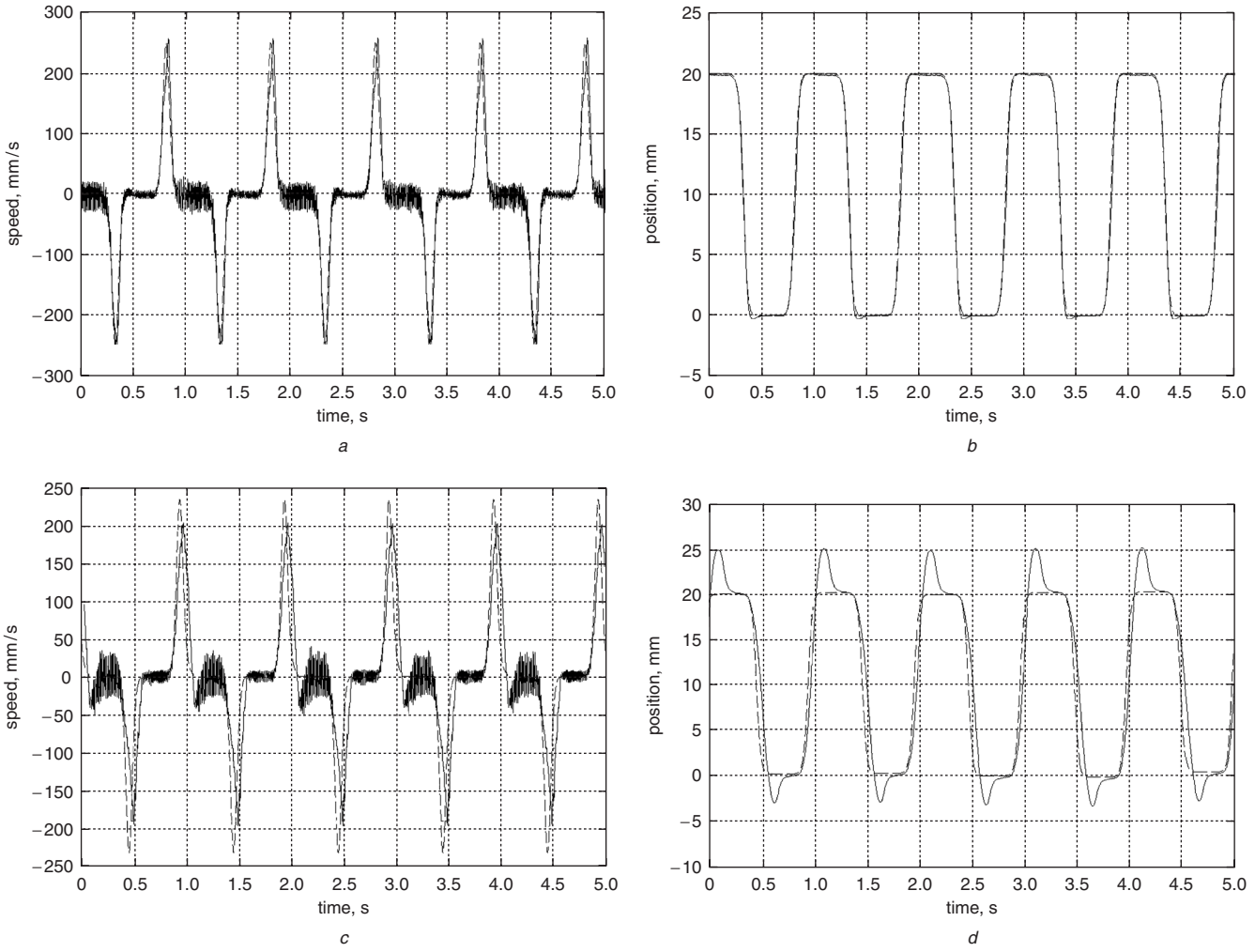

Fig. 9 *Responses of PID controller under 1 Hz, 20 mm*
a Velocity response of x-axis
b Position response of x-axis
c Velocity response of y-axis
d Position response of y-axis

After the force command for each phase is obtained, the required current value can be calculated. Instead of using the lookup table linearisation scheme proposed in [4], a simple linear relationship between force and current is employed [1]. Since the currents supplied to the planar motor are under 15 A for most of the time, and saturation only begins at 18 A or above, a simple linear calculation is adequate. This can reduce memory and processing overhead to the DSP. The force function of current and position is expressed as

$$f(x,i) = \frac{\pi i^2 \Delta L}{P} \sin\left(\frac{2\pi x}{P}\right) \tag{18}$$

where P, x and i are pole pitch, travel distance and phase current, respectively; $2\Delta L$ is the change of phase inductance from aligned to unaligned position. Therefore the reverse relationship of current with force and position can easily be calculated.

Concerning the parameter regulations of an ADRC, the whole system is adjusted empirically on a simulation and experimental basis. The parameters for TD block are based mainly on the arrangement of a proper transient process and the capability of tracking the reference signal successfully within a certain error range. The ESO can be configured according to the 'pole–zero assignment' method above to (i) observe every state of each order and (ii) estimate the whole unpredictable (extended state) precisely. NLSEF decides the stable error and it can be designed on such a basis [15].

The entire control scheme is a typical two dual-rate cascaded loop control. In this paper, the control object is velocity, and the control scheme is ADRC to track the required speed reference signal satisfactorily. To prevent the motor from shifting, a single proportional (P) controller is included for position loop. Figure 5 shows the overall control diagram.

4 Experiment results

A dSPACE DS1104 controller card with a digital signal processor (DSP) clock frequency of 250 MHz is used to implement the controller. The card interfaces with the PC through a PCI bus. Position and velocity feedback signals are collected by optical encoders attached to each axis of movement. The reference current is generated by the controller card and passed on to the digital-to-analogue converters (DACs) and delivered to the current drivers of the motor. The current signal is sensed by current transducers and fed back to the DSP through the analogue-to-digital converters ADCs. Figure 6 shows the overall experimental setup. The whole experiment is operated in real-time; the sampling frequency is 10 kHz

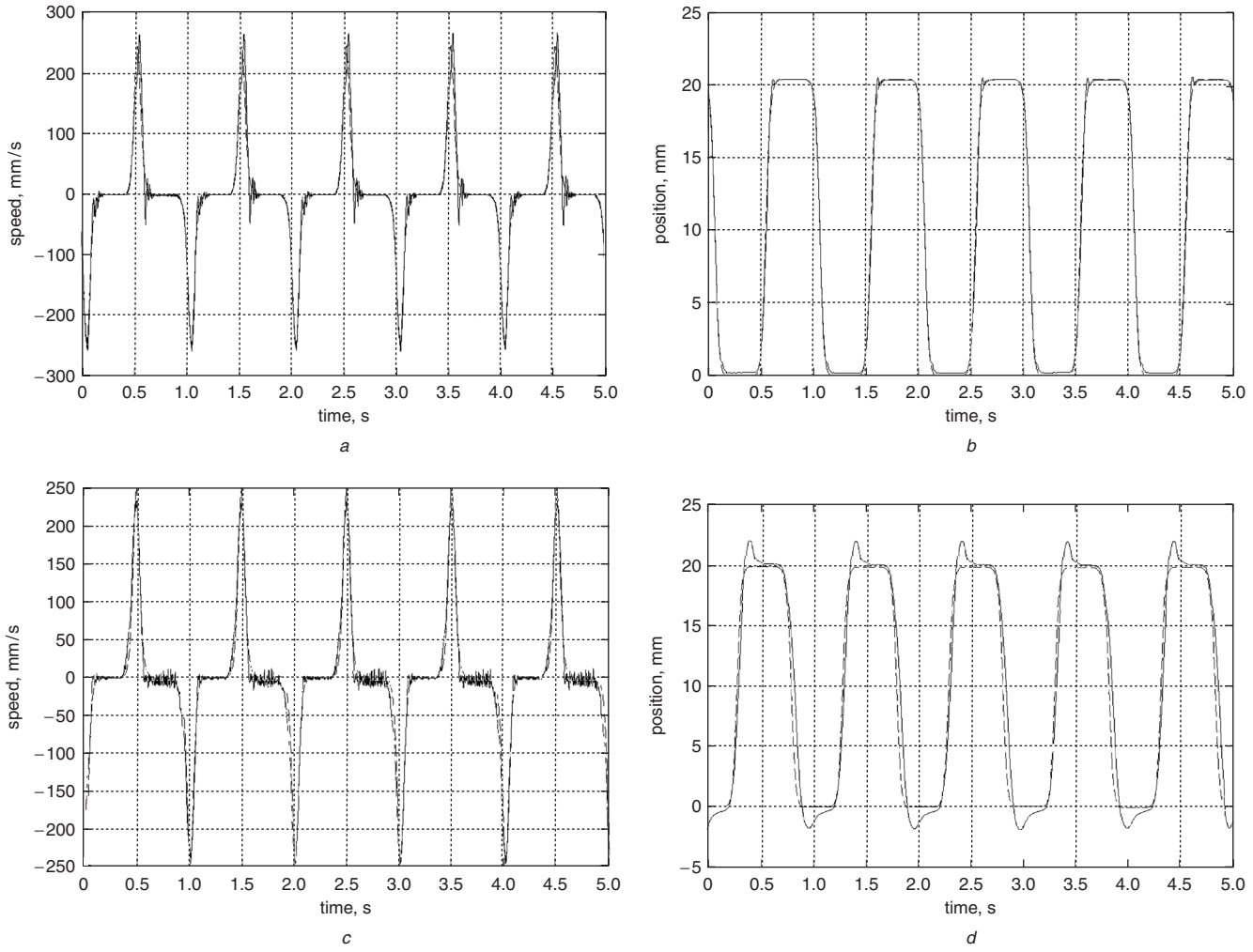

Fig. 10 *Responses of ADRC controller under 1 Hz, 20 mm*
a Velocity response of *x*-axis
b Position response of *x*-axis
c Velocity response of *y*-axis
d Position response of *y*-axis

for the inner current loop and 2 kHz for the outer velocity loop [4].

To avoid undesired oscillatory response, instead of using pure square waveform to test the tracking performance, a quasi third-order S-function [17] signal is used instead. Its profile is directly generated from the tracking differentiator with the input signal as a purely square wave. The TD block can arrange a proper transient process, and the velocity command is obtained from the other output port of the TD. The experiment is mainly focused on the comparisons of speed regulation between a PID controller and the ADRC. It is composed of two parts. The parameters for both controllers according to frequency 0.5 Hz and amplitude 20 mm are regulated and the parameters will remain unchanged. First, the frequency is increased to 1 Hz with amplitude unchanged to observe the motor's behaviour from the two controllers. Second, based on the same parameters (0.5 Hz, 20 mm), some kinds of disturbances are added to the motor to study the responses of both controllers.

The responses of the *x*- and *y*-axis from a PID controller with a position command at 0.5 Hz and amplitude of 20 mm are shown in Fig. 7. The control parameters are shown in Table 2.

There is some noise in velocity responses under PID control for the *x*-axis. Because of the mechanical asymmetry of the motor structure, there exists little positional difference for each direction of movement. Noise also appears in the velocity response under ADRC control scheme (Fig. 8); but compared with the PID controller, the noise is lower and the velocity profile is smooth during zero-crossing regions.

In Fig. 9 the tracking frequency is increased to 1 Hz. Since the mass is much lighter for the *x*-axis mover, the velocity performance is more satisfactory and the response is similar to the 0.5 Hz response. For the *y*-axis, the moving platform cannot track the velocity reference signal correctly and the dynamic error is quite large (Figs. 9*c* and *d*). This is because the *y* moving platform is much heavier and has more inertia. Figure 10 illustrates the motor behaviour under the ADRC control scheme. Both axes have good velocity output performance. It can be concluded that the motor under ADRC is resistant to such model variations.

Next, load disturbances are added to the motor to simulate some real working conditions. Only the *x*-axis is tested. The load disturbances are:

1 Mass change—a steel block of 17.5 N (about 20% of *x* mover) is fixed on the *x*-mover as a whole part.

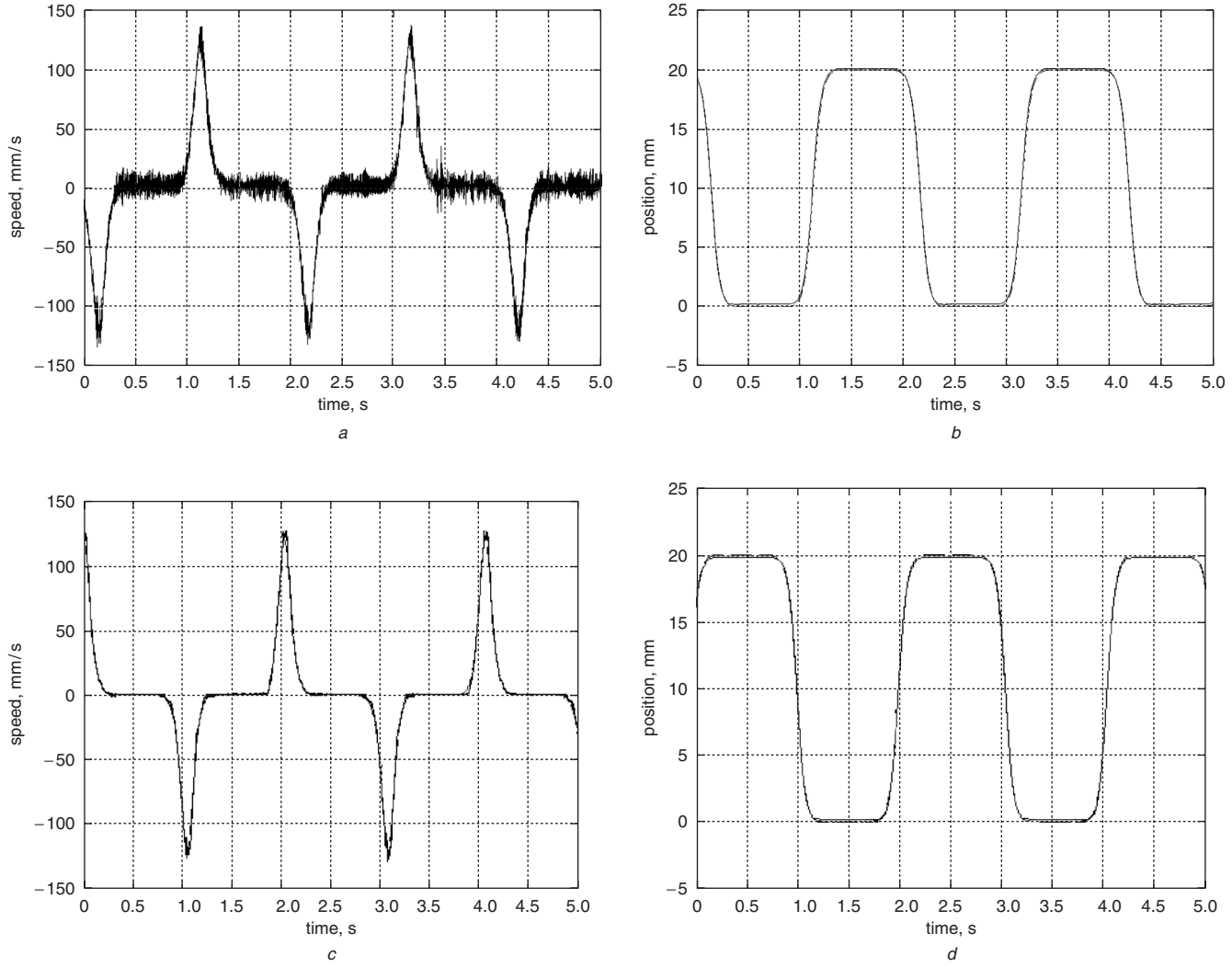

Fig. 11 *Responses of PID and ADRC controller under mass change at 0.5 Hz, 20 mm*
a Velocity response of PID
b Position response of PID
c Velocity response of ADRC
d Position response of ADRC

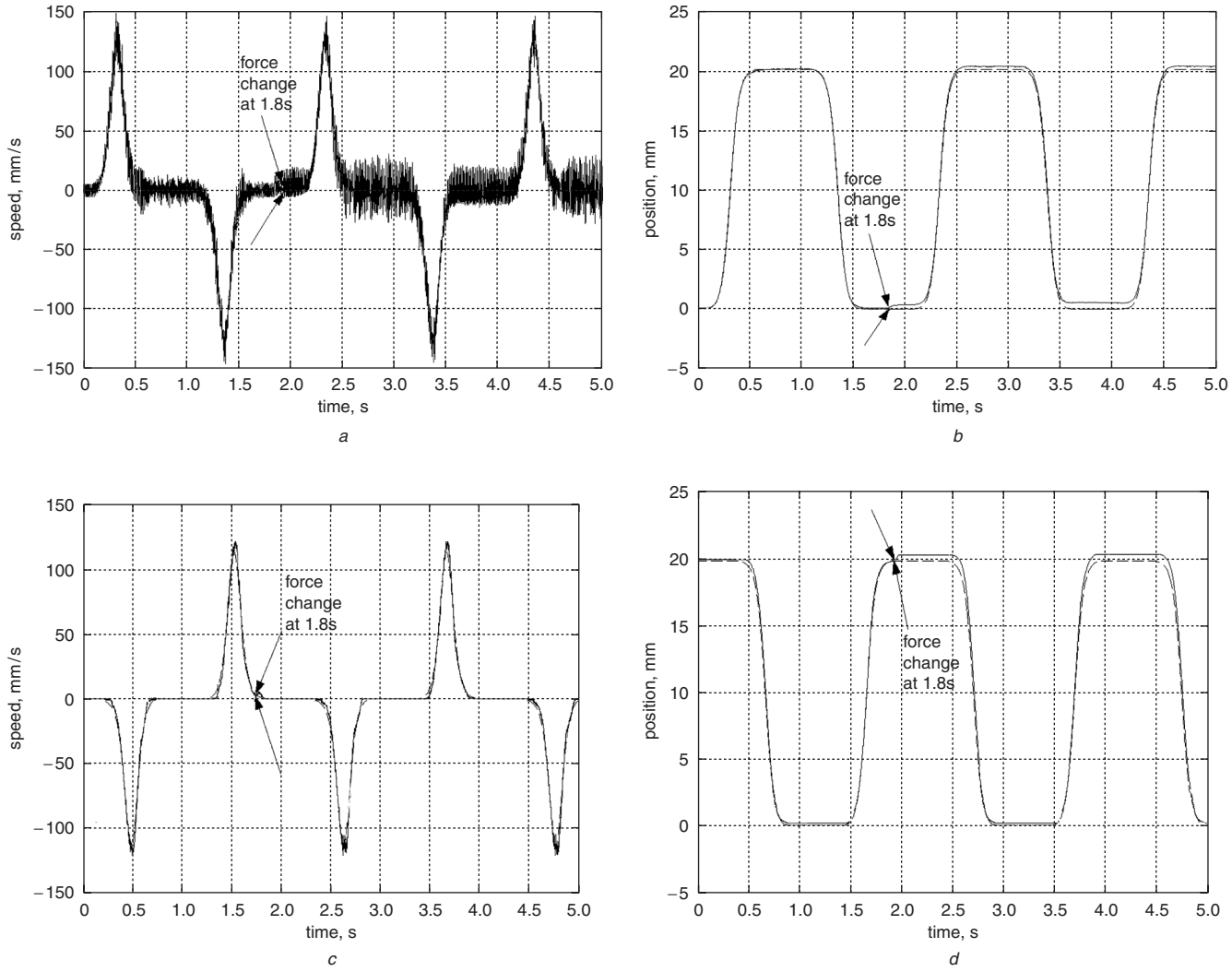

Fig. 12 *Responses of PID and ADRC controller under force variation at time = 1.8 s at 0.5 Hz, 20 mm*
a Velocity response of PID
b Position response of PID
c Velocity response of ADRC
d Position response of ADRC

2 Force disturbance of about 2% is added from the input control command, which occurs at time = 1.8 s.

3 Friction variations with the help of an attached pull-spring (elasticity coefficient of 57.5 N/m).

Figure 11 shows that, for the case of sudden mass change, the ADRC can respond much better than the conventional PID controller.

It can be seen from Fig. 12 that, when force disturbances are introduced, the output performance of velocity becomes worse and the waveform becomes more and more noisy, and it cannot return back to its original conditions. Also, there occurs a positional shift from the actual position of tracking profile. The ADRC controller encounters a velocity dip at time 1.8 s, but the velocity recovers in a very short time. The motor is only under the pull of the spring in one direction of motion, but the force is varied at each position of the mover according to the stator. The velocity response profile in Fig. 13 shows that the speed variations are unbalanced for each direction of motion and the tracking error is much bigger for the PID controller. Therefore the ADRC is more robust in coping with force disturbances.

5 Conclusions

A novel planar motor based on switched reluctance principles has been described. It has many advantages over traditional *x–y* tables. However, the control of the planar motor proposes a new challenge, and normal PID control is inadequate, due to the parameter variations and the direct-drive nature of the motor. In this paper, a model-independent control strategy based on the ADRC principle and the new control scheme has been implemented on the novel planar switched reluctance motor. Compared with the PID control method of the planar motor, in which parameter variations and external disturbances can affect its speed performance, the ADRC is more resistant to uncertainties or disturbances. Therefore the ADRC is a much better choice in controlling the planar SR motor. It is expected that the same method can be applied to control other SR motors with much better robustness than PID control.

The main result from this paper is concentrated on speed regulation with ADRC strategy. It can be seen from the above experimental results that trajectory performance is not well regulated. Therefore, the task ahead will be focused on position control using the ADRC method. It is

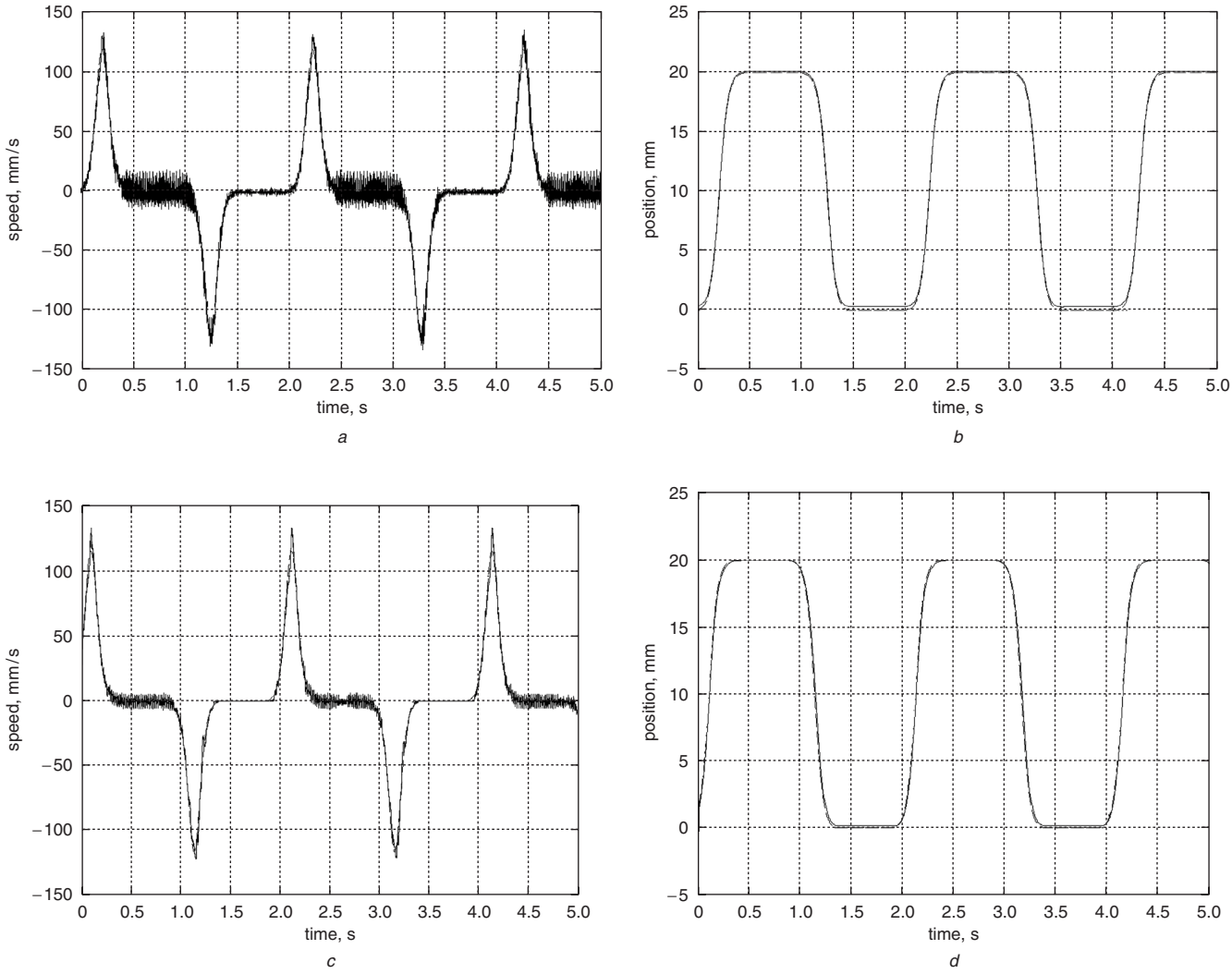

Fig. 13 *Responses of PID and ADRC controller under spring pull at 0.5 Hz, 20 mm*
a Velocity response of PID
b Position response of PID
c Velocity response of ADRC
d Position response of ADRC

worthwhile mentioning that, in a second-order ADRC scheme, parameters to be regulated would be huge. One feasible method under construction is to implement a GA (genetic algorithm) to calculate them online.

6 Acknowledgment

The authors would like to thank the Hong Kong Research Grants Council for sponsoring this research project under the project code B-Q473.

7 References

1 Boldea, I., and Nasar, S.A.: 'Linear electric actuators and generators' (Cambridge University Press, London, UK, 1997)
2 Cheung, N.C., Pan, J.F., and Yang, J.M.: 'Two dimensional variable reluctance planar motor', US Patent (filed: May 2004)
3 Åström, K., Hägglund, T.: 'PID controllers: theory, design and tuning'. Research Triangle Park, NC, USA, International Society of America, USA, 1995
4 Pan, J.F., Cheung, N.C., and Yang, J.M.: 'High-precision position control of a novel planar switched reluctance motor', *IEEE Trans. Ind. Electron.*, (to be published)
5 Gao, Z., Huang, Y., and Han, J.: 'An alternative paradigm for control system design'. Proc. IEEE Conf. on Decision and Control, December 2001, Vol. 5, pp. 4578–4585
6 Su, J., Wenbin *et al.*: 'Calibration-free robotic eye-hand coordination based on an auto disturbance-rejection controller', *IEEE Trans. Robot., Autom*, 2004, **20**, (5), pp. 899–907
7 Jingqing, H.: 'Auto-disturbances-rejection controller and its applications', *Trans. Control Decis., China*, 1998, **13**, (1), pp. 19–23 (in Chinese)
8 Su, Y.X., Duan, B.Y., and Zhang, Y.F.: 'Auto disturbance rejection motion control for direct-drive motors'. Proc. IECON, November 2002, Vol. 3, pp. 2073–2078
9 Wei, S., Wu, B., Qiu, N., and Liu, C.: 'Auto-disturbance rejection controller in direct torque control of permanent magnet synchronous motor drives'. 4th Int. Conf. on Power Electronics and Motion Control (IPEMC), August 2004, Vol. 3, pp. 1268–1272
10 Feng, G., Liu, Y.-F., and Huang, L.: 'A new robust control to improve the dynamic performance of induction motors'. Proc. Power Electronics Specialists Conf. (PESC) 2001, June 2001, Vol. 2, pp. 778–783
11 Xu, L., and Yao, B.: 'Output feedback adaptive robust control of uncertain linear systems with large disturbances'. Proc. American Control Conf., June 1999, Vol. 1, pp. 556–560
12 Su, Y.X., Duan, B.Y., and Zhang, Y.F.: 'Robust precision motion control for AC servo system'. Proc. 4th World Congress on Intelligent Control and Automation, June 2002, Vol. 4, pp. 3319–3323
13 Han, J.-Q., and Wang, W.: 'Nonlinear tracking differentiator', *J. Syst. Sci.Math. Sci.*, 1994, **14**, (2), pp. 177–183 (in Chinese)
14 Jingqing, H.: 'Nonlinear state error feedback control law—NLSEF', *Control Decis.*, 1995, **10**, (3), pp. 221–225 (in Chinese)
15 Jingqing, H.: 'The extended state observer of a class of uncertain systems', *Control Decis., China*, 1995, **10**, (1), pp. 19–23 (in Chinese)
16 Huang, Y., and Han, J.: 'Analysis and design for the second order nonlinear continuous extended states observer', *Chin. Sci. Bull.*, 2000, **45**, (21), pp. 1938–1944 (in Chinese)
17 Gan, W.C., and Cheung, N.C.: 'Development and control of a low-cost linear variable-reluctance motor for precision manufacturing automation', *IEEE/ASME Trans. Mechatronics*, 2003, **8**, (3), pp. 326–333